PHYSICAL REVIEW C **100**, 055804 (2019)

Neutron-star deformation due to anisotropic momentum distribution of neutron-star matter

R. Rizaldy,[1] A. R. Alfarasyi,[2] A. Sulaksono,[1] and T. Sumaryada[2]
[1]*Departemen Fisika, FMIPA, Universitas Indonesia, Depok 16424, Indonesia*
[2]*Departemen Fisika, FMIPA, Institut Pertanian Bogor, Jalan Meranti Kampus IPB Dramaga Bogor 16680, Indonesia*

(Received 25 December 2018; revised manuscript received 12 June 2019; published 26 November 2019)

Herein, we present a theoretical study of how Fermi-surface distortion affects symmetric nuclear matter, pure neutron matter, and neutron-star matter. The results indicate that, for the binding energy of symmetric nuclear matter, the generally accepted value extracted from the Bethe-Weizäcker mass formula for nuclei can constrain the degree of anisotropy because of Fermi-surface deformation $\delta \lesssim 0.05$. The value of δ starts to affect the stiffness of the equation of state for symmetric nuclear matter and pure neutron matter when $\delta \gtrsim 0.01$. Moreover, if the Fermi surface is distorted, the results indicate that neutron stars can be deformed into an oblate shape. This deformation depends on two factors: the stiffness of the corresponding equation of state and value of δ. The corresponding deformation near the maximum neutron-star mass comes from the anisotropic pressure within these stars, which is caused by the distortion of Fermi surface predicted by the equation of state of the models.

DOI: 10.1103/PhysRevC.100.055804

I. INTRODUCTION

Neutron stars (NSs) are excellent objects for studying gravity and dense-matter physics because they are extremely compact and dense with a typical compactness of approximately 0.4 and a density that is several times larger than the nuclear saturation density. However, despite the significant progress made to date, the equation of state (EOS) of high-density nuclear matter remains uncertain, which leads to the degeneracy of the corresponding NS EOSs and use of gravitational theory to describe NSs [1–9].

In the standard picture of nuclear and NS core matter, the quasiparticle momentum distribution is assumed to be homogeneous and isotropic such that the Fermi surface is spherical (i.e., rotationally invariant) with radius k_F. This assumption can be understood from Fermi-liquid theory, which asserts that a system of quasiparticles with the momentum distribution $n_{FL}(k) = \theta(k_F - k)$ remains stable provided any variation $\delta n(k)$ leads to an increase in the energy of the system. However, the distortion or deformation of the Fermi surface can be demonstrated using the Pomeranchuk instability mechanism if the corresponding condition is violated (see Refs. [10–12] and references therein). The phenomenological impact of the distortion or deformation of the Fermi surface appears in diverse branches of physics; therefore, we have reported several studies related to this phenomenon. For example, various studies have investigated the impact of the deformation of the Fermi surface in a bipolar Fermi gas [13], trapped Fermi gases with different spin populations [14], and ultracold Fermi gas atoms [15]. Moreover, the pressure-induced Fermi-surface deformation in lithium and its relation to the observed complexity behavior were investigated [16]. In addition, a homogeneous superconductor with broken spin-isospin symmetry has been shown to lower its energy by transitioning to a novel superconducting state where the Fermi surfaces are deformed to a quasiellipsoidal form at zero total momentum of the corresponding Cooper pairs [17]. In another study, the phases of asymmetric nuclear matter with broken space symmetries were studied [18]. The impact of the Fermi-surface deformation induced by interactions in the momentum distribution of spin-polarized asymmetric nuclear matter was investigated in Ref. [19] (see references therein for details). Other studies have reported the local anisotropy in post-Newtonian gravity, which is caused by the distortion of the Fermi surface of the electron gas and the application of this matter in white dwarfs and supermassive stars [20]. To simplify the picture, it is usually assumed that the baryons, which are the constituents of the symmetric nuclear matter (SNM), pure neutron matter (PNM), and NS matter, are point particles. Baryons are composite particles composed of three quarks; therefore, we expect that, through the excluded-volume effect, the compositeness of the corresponding baryons in nuclear or NS matter would macroscopically manifest itself as an inhomogeneous distribution of matter. Furthermore, this inhomogeneity effect may distort the appearance of the Fermi surface. In Ref. [21], we discuss how the excluded volume affects the properties of SNM, PNM, and slow-rotating NSs.

In this study, we use an approach similar to that of Refs. [19,20] to study how the distortion of the Fermi surface of nucleon gas affects the SNM, PNM, and NS matter. We assume that the Fermi momentum of matter depends on the polar angle θ, which is the angle between the z axis and the radial direction in spherical coordinates. In fact, the Fermi momentum k_f is calculated using the following equation:

$$k_f(\theta) \equiv k_f[1 + \delta P_2(\cos\theta)]. \tag{1}$$

Equation (1) describes the shape deformation up to quadrupole order. $P_2(\cos\theta)$ is the Legendre polynomial with $l = 2$ and δ is a parameter that measures the degree of anisotropy because of Fermi-surface distortion [the surface of objects may be described quite generally by an expansion in spherical harmonics $Y_l^m(\theta, \phi)$]. For example, for a nucleus [22], the $l = 0$ term is the monopole term, which is associated with the breathing mode; the $l = 1$ term is the dipole term, which has no relation to shape deformation; and the $l = 2$ term is related to quadrupole deformation. The expansion to $l = 2$ and $m = 0$ is sufficient to describe nuclei with azimuthal symmetry, such as nuclei of prolate or oblate shape. Similarly, we need to consider up to $l = 2$ to describe the Fermi-surface deformation up to the quadrupole term.

To estimate the allowed value of δ, we used the range of SNM and PNM EOSs extracted from experimental heavy-ion-collision data, the accepted SNM binding energy extracted from the Bethe-Weizäcker mass formula for nuclei, and the range of SNM binding energy for the region extracted from FOPI experimental data near twice the saturation density. Furthermore, we investigate how the allowed value of δ affects the stiffness of the EOS of the SNM and PNM at relatively high densities and the corresponding NS properties.

In Sec. II, we briefly discuss the formalism used to calculate the EOS, which involves the relativistic mean-field (RMF) approach and the corresponding NS properties. In Sec. III, we present and discuss the results. In Sec. IV, we summarize the conclusions of this investigation.

II. FORMALISM

In this section, we briefly discuss the formalism that was used to calculate the EOS of SNM, PNM, and NS matter. This formalism considers the angle dependence of the Fermi momentum defined in Eq. (1) within the RMF approach. Moreover, we present the formalism used to calculate NS properties, including deformation, where we use an approach introduced by Hartle and Thorne [23–25].

A. Model of nuclear and neutron-star matter

The Lagrangian density of the RMF model is given by the following equation [7]:

$$\mathcal{L} = \mathcal{L}_N + \mathcal{L}_M + \mathcal{L}_{\text{int}}, \tag{2}$$

where the contribution of free nucleons is

$$\mathcal{L}_N = \sum_N \overline{\psi}_N (i\gamma_\mu \partial^\mu - M_N)\psi_N, \tag{3}$$

with the sum taken over all nucleons (protons and neutrons). Note that the interactions between nucleons are mediated by the exchange of scalar, vector, and isovector (σ, ω, and ρ, respectively) mesons, which also have self-interactions; therefore, the interaction terms are as follows [26]:

$$\begin{aligned}\mathcal{L}_{\text{int}} = {} & \sum_N g_\sigma \sigma \overline{\psi}_N \psi_N - \sum_N g_\omega V_\mu \overline{\psi}_N \gamma^\mu \psi_N \\ & - \sum_N g_\rho \mathbf{b}_\mu \overline{\psi}_N \gamma^\mu \boldsymbol{\tau} \psi_N - \frac{1}{3} b_2 \sigma^3 - \frac{1}{4} b_3 \sigma^4 + \frac{1}{4} c_3 (V_\mu V^\mu)^2 \\ & + d_2 \sigma (V_\mu V^\mu) + f_2 \sigma (\mathbf{b}^\mu \mathbf{b}_\mu) + \frac{1}{2} d_3 \sigma^2 (V_\mu V^\mu).\end{aligned} \tag{4}$$

For free mesons, the Lagrangian density takes the following form:

$$\mathcal{L}_M = \mathcal{L}_\sigma + \mathcal{L}_\omega + \mathcal{L}_\rho, \tag{5}$$

where

$$\mathcal{L}_\sigma = \tfrac{1}{2}\left(\partial_\mu \sigma \partial^\mu \sigma - m_\sigma^2 \sigma\right), \tag{6}$$

$$\mathcal{L}_\omega = -\tfrac{1}{2}\left(\tfrac{1}{2}\omega_{\mu\nu}\omega^{\mu\nu} - m_\omega^2 V_\mu V^\mu\right), \tag{7}$$

$$\mathcal{L}_\rho = -\tfrac{1}{2}\left(\tfrac{1}{2}\boldsymbol{\rho}_{\mu\nu}\boldsymbol{\rho}^{\mu\nu} - m_\rho^2 \mathbf{b}_\mu \mathbf{b}^\mu\right). \tag{8}$$

Within the mean-field approximation, σ, $V^\mu(V_0, 0)$, and $\mathbf{b}^\mu(\mathbf{b}_0, 0)$ are σ, ω, and ρ fields, respectively, and $\omega_{\mu\nu}$ and $\boldsymbol{\rho}_{\mu\nu}$ are the antisymmetric tensors of ω and ρ meson fields. Because NS matter should obey the β-stability condition, leptons should appear in the NS matter. The contribution of noninteracting leptons (i.e., electrons and muons) to the total Lagrangian density is as follows:

$$\mathcal{L}_L = \sum_L \overline{\psi}_L (i\gamma_\mu \partial_\mu - m_L)\psi_L. \tag{9}$$

To simplify the problem, we assume that the Fermi surface of leptons is not distorted; therefore, the expression for the zero component of the vector (lepton number) density and the energy density and pressure derived from Eq. (9) take the standard forms [27].

Using the RMF calculation procedure [27], we obtained the following nucleon number densities for matter with a distorted Fermi surface:

$$\rho_N^* = 2\int_0^{k_f^N(\theta)} \frac{d^3k}{(2\pi)^3}, \quad N = p, n. \tag{10}$$

Similarly, scalar number densities for protons and neutrons are expressed as follows:

$$\rho_{sN}^* = 2\int_0^{k_f^N(\theta)} \frac{M_N^*}{\sqrt{k^2 + M_N^{*2}}} \frac{d^3k}{(2\pi)^3}, \tag{11}$$

where $M_N^* = M_N + g_\sigma \sigma$. The total energy density can be calculated as follows:

$$\begin{aligned}\epsilon = {} & \sum_{N=n,p} \epsilon_N^* + g_\omega(\rho^p + \rho^n) \\ & + \frac{1}{2} g_\rho (\rho^p - \rho^n) + U + \sum_{L=e,\mu} \epsilon_L,\end{aligned} \tag{12}$$

where the meson contribution is as follows:

$$\begin{aligned}U = {} & \tfrac{1}{2} m_s^2 \sigma^2 - \tfrac{1}{2} m_\omega^2 V_0^2 + \tfrac{1}{2} m_\rho^2 b_0^2 \\ & + \tfrac{1}{3} b_2 \sigma^3 + \tfrac{1}{4} b_3 \sigma^4 - \tfrac{1}{4} c_1 V_0^4 \\ & - d_2 \sigma V_0^2 - f_2 \sigma b_0^2 - \tfrac{1}{2} d_3 \sigma^2 V_0^2,\end{aligned} \tag{13}$$

and the nucleon contributions are as follows:

$$\epsilon_N^* = \frac{1}{4\pi^3} \int_0^{k_f^N(\theta)} \sqrt{k^2 + M_N^{*2}}\, d^3k. \tag{14}$$

The distortion of the Fermi surface leads to unequal pressure in the tangential (P_t) and radial (P_r) directions. The explicit expressions for P_t and P_r are as follows:

$$P_{r/t} = \sum_{M=n,p} \frac{1}{3} P^{*N}_{r/t} - U + \sum_{L=e,\mu} \frac{1}{3} P_L, \tag{15}$$

with [20]

$$\begin{aligned} P^{*N}_r &= \frac{1}{4\pi^3} \int_0^{k_f^N(\theta)} cos^2(\theta) \frac{k^2}{\sqrt{k^2 + M_N^{*2}}} d^3k, \\ P^{*N}_t &= \frac{1}{4\pi^3} \int_0^{k_f^N(\theta)} \frac{1}{2}[1 - cos^2(\theta)] \frac{k^2}{\sqrt{k^2 + M_N^{*2}}} d^3k. \end{aligned} \tag{16}$$

In Sec. II B, we discuss the approximation of the corresponding densities, energy density, and pressures, all of which are useful for the proposed application.

B. Approximation of anisotropic momentum distribution in matter

The number density can be expressed exactly; therefore, the explicit form of Eq. (10) is as follows:

$$\rho_N^* = \left[\frac{1}{3\pi^2} k_f^{N\,3} + \frac{1}{105\pi^2} ((2\delta + 21)\delta^2) k_f^{N\,3} \right], \tag{17}$$

where the second term appears because of the Fermi-surface distortion, which includes terms up to third order in δ. Other densities and pressures cannot be exactly expressed in analytical forms; however, they can be approximated by expanding the solution in powers of δ (we assume that δ is a small number). Therefore, to be consistent with the expression for ρ_N^*, we included only up to third order in δ for other quantities. Note that scalar number densities of nucleons [Eq. (11)] can be analytically expressed as follows:

$$\rho_{sN}^* = \rho_{sN} + \Delta\rho_{sN}(\delta), \tag{18}$$

with

$$\rho_{sN} = \frac{M_N^*}{2\pi^2} \left\{ k_F^N \sqrt{k_F^{N^2} + M_N^{*^2}} - M_N^{*^2} \ln \left[\frac{k_F^N + \sqrt{k_F^{N^2} + M_N^{*^2}}}{M_N^*} \right] \right\}, \tag{19}$$

and

$$\Delta\rho_{sN}(\delta) \approx \frac{1}{\pi^2} \left\{ \delta^2 \left[\frac{k_f^{N\,3}}{5} + \frac{9k_f^{N\,7}}{40M_N^{*^4}} + \frac{k_f^{N\,5}}{5M_N^{*^2}} \right] + \delta^3 \left[\frac{2k_f^{N\,3}}{105} + \frac{3k_f^{N\,7}}{28M_N^{*\,4}} + \frac{2k_f^{N\,5}}{35M_N^{*\,2}} \right] \right\}. \tag{20}$$

The first expression is summed over all orders of k_f^N/M_N^*; however, based on the assumption that $k_f^N/M_N^* < 1$, the second expression is obtained by expanding the exact integral expressions and retaining up to third order in δ. We retained only the leading-order terms of k_f^N/M_N^*. Using an approximation similar to that used for expressing nucleon energy densities, $\Delta\rho_{sN}(\delta)$ [Eq. (14)], we obtain

$$\epsilon_N^* = \epsilon_N + \Delta\epsilon_N(\delta), \tag{21}$$

with

$$\epsilon_N = \frac{1}{8\pi^2} \left\{ k_f^N \sqrt{k_f^{N\,2} + M_N^{*^2}} \left(2k_f^{N\,2} + M_N^{*\,2} \right) - M_N^{*\,4} \ln \left[\frac{k_f^N + \sqrt{k_f^{N\,2} + M_N^{*\,2}}}{M_N^*} \right] \right\}, \tag{22}$$

and

$$\Delta\epsilon_N(\delta) \approx \frac{1}{\pi^2} \left\{ \delta^2 \left[\frac{-3k_f^{N\,7} + 8k_f^{N\,5} M_N^{*^2} + 8k_f^{N\,3} M_N^{*^4}}{40M_N^{*^3}} \right] + \delta^3 \left[\frac{-15k_f^{N\,7} + 24k_f^{N\,5} M_N^{*^2} + 8k_f^{N\,3} M_N^{*^4}}{420M_N^{*^3}} \right] \right\}. \tag{23}$$

For a spherical Fermi surface ($\delta = 0$), radial pressure P_r and tangential pressure P_t of the nucleon matter are the same (i.e., $P = P_r = P_t$). However, for a distorted Fermi surface, $P_r \neq P_t$ and the average pressure (or θ-independent pressure) P is as follows:

$$P = \tfrac{1}{3}(P_r + 2P_t). \tag{24}$$

When the deformation of the Fermi surface is considered, the radial and tangential pressures can be calculated as follows:

$$P^{*N}_{r/t} = P^N + \Delta P^N_{r/t}(\delta), \tag{25}$$

where the nucleon isotropic pressure is as follows:

$$P^N = \frac{1}{8\pi^2} \left\{ k_f^N \sqrt{k_f^{N\,2} + M_N^{*\,2}} \left(2k_f^{N\,2} - 3M_N^{*\,2} \right) + 3M_N^{*\,4} \ln \left[\frac{k_f^N + \sqrt{k_f^{N\,2} + M_N^{*\,2}}}{M_N^*} \right] \right\}, \tag{26}$$

and the correction for radial pressure is as follows:

$$\Delta P_r^N(\delta) \approx \frac{\left(3k_f^{N\,9} - 4k_f^{N\,7} M_N^{*^2} + 8k_f^{N\,5} M_N^{*^4}\right)\delta}{20M_N^{*^5}\pi^2} + \frac{11\left(3k_f^{N\,9} - 3k_f^N 7M_N^{*^2} + 4k_f^{N\,5} M_N^{*^4}\right)\delta^2}{70M_N^{*^5}\pi^2} + \frac{4\left(7k_f^{N\,9} - 5k_f^N 7M_N^{*^2} + 4k_f^{N\,5} M_N^{*^4}\right)\delta^3}{35M_N^{*^5}\pi^2}, \tag{27}$$

while the correction for tangential pressure is as follows:

$$\Delta P_t^N(\delta) \approx \frac{\left(-3k_f^{N^9} + 4k_f^{N^7} M_N^{*^2} - 8k_f^{N^5} M_N^{*^4}\right)\delta}{40 M_N^{*^5}\pi^2} + \frac{\left(3k_f^{N^9} - 3k_f^N 7 M_N^{*^2} + 4k_f^{N^5} M_N^{*^4}\right)\delta^2}{14 M_N^{*^5}\pi^2} + \frac{\left(-7k_f^{N^9} + 5k_f^N 7 M_N^{*^2} - 4k_f^{N^5} M_N^{*^4}\right)\delta^3}{70 M_N^{*^5}\pi^2}. \qquad (28)$$

Based on these pressures and energy densities, and assuming we know the Fermi momentum of each constituent, we can calculate the EOSs of each corresponding type of matter. Note that, for PNM, we only required k_f^n to determine the EOS whereas we need $k_f^n = k_f^p$ as input to calculate the EOS for SNM. However, for the EOS of the NS core, we need to apply β stability and the neutrality conditions to determine the Fermi momentum of each constituent. Moreover, for the NS matter, we assume only that it is composed of nucleons and leptons. To simplify our calculation, we average out over a complete solid angle the corresponding θ dependence of the Fermi momentum given the β stability and neutrality conditions such that $\langle k_f(\theta)\rangle = k_f$. In this manner, we obtain $k_f = [C(\delta)\rho]^{1/3}$ with $C(\delta) = \frac{105\pi^2}{[35+\delta^2(21+2\delta)]}$. The following approximate forms of the conditions are used to determine the Fermi momentum of each constituent:

(i) Neutrality

$$\langle \rho^p \rangle = \rho^e + \rho^\mu.$$

(ii) β stability

$$\sqrt{k_F^{\mu^2} + m_\mu^2} = \sqrt{\langle k_F^{n^2}(\theta)\rangle + M_n^{*^2}} - \sqrt{\langle k_F^{p^2}(\theta)\rangle + M_p^{*^2}} + g_\rho b_0,$$

$$\sqrt{k_F^{e^2} + m_e^2} = \sqrt{\langle k_F^{n^2}(\theta)\rangle + M_n^{*^2}} - \sqrt{\langle k_F^{p^2}(\theta)\rangle + M_p^{*^2}} + g_\rho b_0.$$

(iii) Nucleon density

$$\rho = \langle \rho^p \rangle + \langle \rho^n \rangle. \qquad (29)$$

In each constituent, the superscripts $p, n, e,$ and μ of the Fermi momenta and densities indicate that the given quantity corresponds to protons, neutrons, electrons, and muons, respectively.

C. Neutron-star deformation because of distorted Fermi surface

If we define the anisotropic pressure factor σ as follows:

$$\sigma \equiv P_r - P_t, \qquad (30)$$

then we can write P_r and P_t as a function of average pressure P and σ [Eq. (24)]:

$$P_r = P + \tfrac{2}{3}\sigma, \qquad (31)$$

$$P_t = P - \tfrac{1}{3}\sigma, \qquad (32)$$

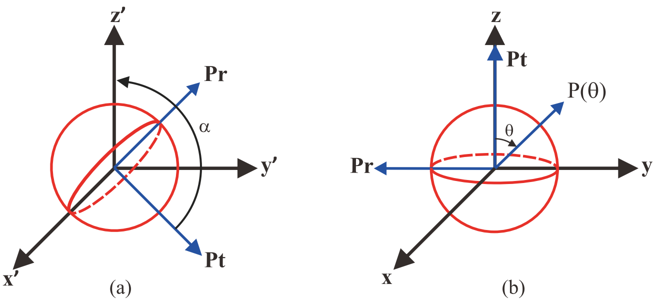

FIG. 1. Illustration of adjusting the coordinates of NS pressures (a) original coordinates and (b) coordinates after rotation.

and the anisotropic energy-momentum tensor can be expressed as follows:

$$T_{\mu\nu} = \begin{pmatrix} -\epsilon & 0 & 0 & 0 \\ 0 & P_r & 0 & 0 \\ 0 & 0 & P_t & 0 \\ 0 & 0 & 0 & P_t \end{pmatrix}. \qquad (33)$$

As shown in Fig. 1, if we rotate P_t by an arbitrary angle α from the original coordinates (x', y', z') such that in new coordinates (x, y, z) P_t is in z axes and P_r is in x-y plane, the total pressure in new coordinates can be defined as a function of θ, $P(\theta)$ such that if we rotate the $P(\theta)$ into z axes, $P(0) = P_t$. Moreover, if rotate $P(\theta)$ into x-y plane, $P(3\pi/2) \equiv P(\pi/2) = P_r$, and the latter satisfies the condition because we selected $P(\theta)$ as an even function. Using this procedure, we can express Eq. (33) as an isotropic form of $T_{\mu\nu}$ but with the θ dependence of the total pressure $P(\theta)$ [25] by defining the total pressure as follows:

$$P(\theta) \equiv P + p_0 + p_2 P_2(\cos\theta), \qquad (34)$$

with $p_0 = \sigma/3$ and $p_2 = -2\sigma/3$. Note that Eq. (34) reduces to Eqs. (31) and (32) if we substitute $\theta = \pi/2$ and $\theta = 0$ into $P(\theta)$, respectively. Note that the choice of α is rather arbitrary; therefore, the results depend on the selected coordinates. For example, we can also choose other value of α such that $P(0) = P_r$ and $P(\pi/2) = P_t$. In these coordinates, we should use the different value of p_0 and p_2. The physics is the same but the interpretation of the results is coordinate dependent. In this manner, we can write the energy-momentum tensor in the following isotropic form:

$$T_{\mu\nu} = \begin{pmatrix} -\epsilon & 0 & 0 & 0 \\ 0 & P(\theta) & 0 & 0 \\ 0 & 0 & P(\theta) & 0 \\ 0 & 0 & 0 & P(\theta) \end{pmatrix}. \qquad (35)$$

For a spherical NS, we use the Schwarzschild metric as follows:

$$ds^2 = -e^{\nu(r)}dt^2 + e^{\lambda(r)}dr^2 + r^2(d\theta^2 + \sin^2\theta d\phi^2), \qquad (36)$$

where $\nu(r)$ and $\lambda(r)$ are the metric functions. Because we assume that the anisotropic pressure only perturbatively distorts the spherical shape, we can express the metric of a deformed NS by modifying the Schwarzschild metric using the multipole expansion introduced by Hartle and Thorne

[23,24]. In this approach, ds^2 can be expressed as follows:

$$\begin{aligned} ds^2 =& -e^{\nu(r)}[1+2H(r,\theta)]dt^2 \\ &+ e^{\lambda(r)}\left[1+\frac{2e^{\lambda(r)}}{r}m(r,\theta)\right]dr^2 \\ &+ r^2[1+2K(r,\theta)](d\theta^2+\sin^2\theta d\phi^2), \end{aligned} \tag{37}$$

where

$$\begin{aligned} H(r,\theta) &= h_0(r)+h_2(r)P_2(\cos\theta)+\dots, \\ m(r,\theta) &= m_0(r)+m_2(r)P_2(\cos\theta)+\dots, \\ K(r,\theta) &= k_0(r)+k_2(r)P_2(\cos\theta)+\dots. \end{aligned} \tag{38}$$

Here, $k_0(r)=0$ [23] because the form of the metric should not change under a coordinate transformation. To be consistent with the expansion of the momentum-energy tensor, which only includes up to the quadrupole order ($l=2$), the multipole expansion of the Schwarzschild metric is truncated at quadrupole order. In this approximation, ds^2 simplifies to

$$\begin{aligned} ds^2 =& -e^{\nu(r)}\{1+2[h_0(r)+h_2(r)P_2(\cos\theta)]\}dt^2 \\ &+ e^{\lambda(r)}\left[1+\frac{2e^{\lambda(r)}}{r}[m_0(r)+m_2(r)P_2(\cos\theta)]\right]dr^2 \\ &+ r^2\{1+2[k_2(r)P_2(\cos\theta)]\}(d\theta^2+\sin^2\theta d\phi^2). \end{aligned} \tag{39}$$

We can now solve the Einstein field equations by separating the solutions according to the leading-order terms and those from the multipole expansion (i.e., the $l=0$ and $l=2$ terms, respectively). The following gives the expressions for the Einstein field equations to leading order and includes the correction because of the multipole expansion:

$$\begin{aligned} G^\mu_\nu &= 8\pi G T^\mu_\nu \\ \Delta G^\mu_\nu &= 8\pi G \Delta T^\mu_\nu, \end{aligned} \tag{40}$$

where $\Delta G^\mu_\nu = \Delta_0 G^\mu_\nu + \Delta_2 G^\mu_\nu$ and $\Delta T^\mu_\nu = \Delta_0 T^\mu_\nu + \Delta_2 T^\mu_\nu$. From the first of Eqs. (40) (i.e., the leading-order equation), we obtain the unperturbed spherical contribution, which yields the standard Tolman-Oppenheimer-Volkoff equations for spherical stars:

$$P' = -\frac{G\epsilon m}{r^2}\frac{\left[1+\frac{P}{\epsilon}\right]\left[1+4\pi r^3\frac{P}{m}\right]}{\left[1-2\frac{Gm}{r}\right]} \tag{41}$$

$$m' = 4\pi r^2\epsilon, \tag{42}$$

where the prime in Eq. (42) indicates a derivative with respect to r. Equation (42) can be numerically solved by using the boundary conditions $m(0)\approx 0$, $m(R)\approx M_0$, and $P(R)\approx 0$, $P(0)\approx P_c$. Here, P_c is the pressure at the center of the NS, R is the radius of the spherical NS, and M_0 is the mass of the spherical NS. The first part of the second of Eqs. (40) ($\Delta_0 G^\mu_\nu = 8\pi\Delta_0 T^\mu_\nu$) is the monopole correction, and the second part ($\Delta_2 G^\mu_\nu = 8\pi\Delta_2 T^\mu_\nu$) is the quadrupole correction. For the monopole correction, we obtain $\Delta_0 G^r_r = 8\pi\Delta_0 T^r_r$ and $\Delta_0 G^t_t = 8\pi\Delta_0 T^t_t$. Both relations can be further simplified, with the final results being

$$h_0' = \left[4\pi G r p_0 + \frac{Gm_0}{r}\left(\nu'+\frac{1}{r}\right)\right]e^\lambda \quad m_0' = 0. \tag{43}$$

Clearly because m_0 is zero at the center, m_0 becomes zero everywhere. For the quadrupole correction, we obtain $\Delta_2 G^r_r = 8\pi\Delta_2 T^r_r$, $\Delta_2 G^\theta_\theta = \Delta_2 G^\phi_\phi$, and $G^\theta_r = 0$. These equations are then further simplified to

$$\begin{aligned} h_2 + \frac{e^\lambda}{r}Gm_2 &= 0 \\ h_2' + k_2' + \frac{r}{2}\nu' k_2' &= 4\pi G r e^\lambda p_2 + \frac{e^\lambda}{r^2}Gm_2 \\ &\quad + \frac{e^\lambda}{r}Gm_2\nu' + \frac{3}{r}e^\lambda h_2 + \frac{2}{r}e^\lambda k_2 \\ h_2' + k_2' &= h_2\left(\frac{1}{r}-\frac{\nu'}{2}\right) + \frac{e^\lambda}{r}Gm_2\left(\frac{1}{r}+\frac{\nu'}{2}\right). \end{aligned} \tag{44}$$

Note that the expressions for h_0', h_2', and k_2' in Eqs. (43) and (44) are quite complicated; however, we can obtain much simpler versions of these relations from energy-momentum conservation using the Bianchi identity. For the leading order, we have the following:

$$P' = -\frac{(P+\epsilon)}{2}\nu', \tag{45}$$

for the monopole correction, we have the following:

$$p_0' = -\tfrac{1}{2}\nu' p_0 - (P+\epsilon)h_0', \tag{46}$$

and for the quadrupole correction, we have the following:

$$p_2 = -(P+\epsilon)h_2 \tag{47}$$

$$p_2' = -\tfrac{1}{2}\nu' p_2 - (P+\epsilon)h_2'. \tag{48}$$

We can simplify the last two equations into expressions for k_2' and h_2' using Eqs. (44), (47), and (48), which gives the following more compact expressions for k_2' and h_2':

$$k_2' = \frac{\frac{3}{2}p_2\nu' + p_2'}{P+\epsilon} \tag{49}$$

$$h_2' = \frac{-\frac{1}{2}p_2\nu' - p_2'}{P+\epsilon}. \tag{50}$$

To simplify the numerical calculation, we considered solving Eqs. (41), (42), (46), (49), and (50) numerically using $p_2 = -2p_0$. Consequently, we obtained the profile of P, ϵ, m, p_0, p_2, h_0, and k_2 for each central energy density. These results are used to describe the deformations occurring in the NSs because of anisotropic pressure caused by the distorted Fermi surface. Note that the boundary conditions used to solve Eqs. (49) and (50) are $h_0(0)\approx 0$ and $k_2(0)\approx 0$.

These differential equations, which were obtained from the Einstein field equations, are quite similar to those obtained in Refs. [23,28], which considered deformation because of slow rotation, and to those of Ref. [25], which considered deformation because of a magnetic field. Note that no factor of $\frac{1}{2}$ appears in Eq. (46) because the energy density in the expression ϵ for matter does not include $l=0$ (monopole) or $l=2$ (quadrupole) correction terms. This is in stark contrast with the corresponding total pressure where we obtain monopole p_0 and quadrupole p_2 terms because of the deformed Fermi surface [see Eq. (34)].

Following Refs. [23,24], we define the NS radius as a general function of θ:

$$r(r,\theta) = r + \xi_0(r) + [\xi_2(r) + rk_2(r)]P_2(\cos\theta), \tag{51}$$

where ξ_l is:

$$\xi_l(r) = \frac{(P+\epsilon)}{P'}h_l(r). \tag{52}$$

Here $l = 0$ (2) denotes the monopole (quadrupole) contribution. From Eq. (51), we obtain two types of radii to locate the edge of a deformed NS, i.e., the equatorial and polar radii. These are given by the following equations:

$$R_e = R + \xi_0(R) - \tfrac{1}{2}[\xi_2(R) + Rk_2(R)] \tag{53}$$

$$R_p = R + \xi_0(R) + [\xi_2(R) + Rk_2(R)]. \tag{54}$$

Finally, the degrees of deformation are obtained from the eccentricity, which is expressed as follows:

$$e = \sqrt{1 - \left(\frac{R_p}{R_e}\right)^2}. \tag{55}$$

The mass of a deformed NS is $M = M_0 + m_0(R)$. Note that the deformation factors are easily identified if we know ϵ and σ as a function of P, which we calculate by applying the RMF approach to the NS core, whereas we use the same EOS as used in Ref. [21] for the NS crust. In our calculation, we use the NL3 [29], TM1 [30], and G2 [31] parameter sets to represent stiff, moderate, and soft EOSs. A detailed discussion of the properties of the SNM, PNM, and NS matter predicted by the NL3, TM1, and G2 parameter sets and the tabulation of the parameter values can be found in Refs. [7,29–31]. Furthermore, we vary the δ value and use all representative EOSs to study how the EOS stiffness affects NS deformation through a distorted Fermi surface.

III. RESULTS AND DISCUSSIONS

In this section, we discuss how the distorted Fermi surface affects the SNM, PNM, and NS matter, as well as the NS properties.

A. Impact of distorted Fermi surface on nuclear matter

The top panels of Figs. 2–4 show the pressure as a function of the ratio of nucleon density to nuclear saturation density of SNM (ρ_N/ρ_0). The bottom panels show the SNM binding energy as a function of nucleon density at moderate density. The bottom and top panels of Figs. 5–7 show the PNM pressure as a function of ρ_N/ρ_0 as well as the PNM binding energy as a function of neutron density in the low-density region. The

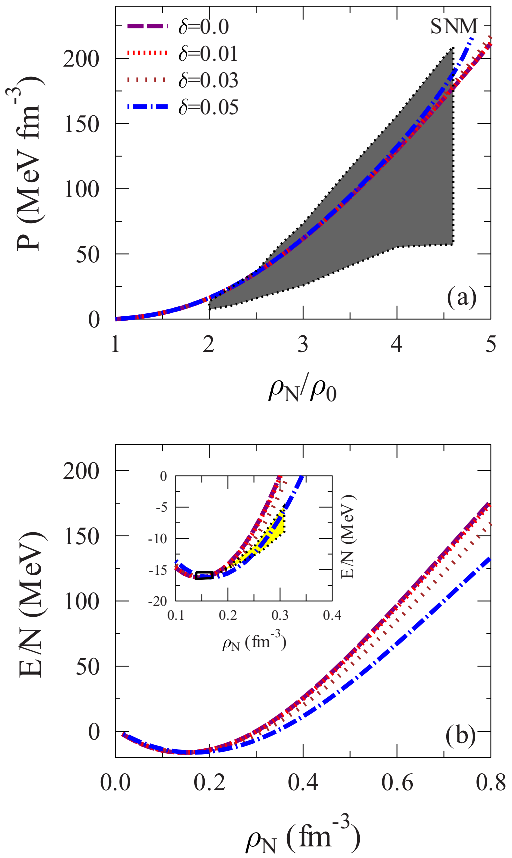

FIG. 2. (a) Pressure as a function of the ratio of nucleon-to-nuclear saturation densities. (b) Energy per particle as a function of the density around the saturation density for SNM with different δ values obtained from TM1 parameter set. The dashed curves correspond to various numbers δ deformation, respectively.

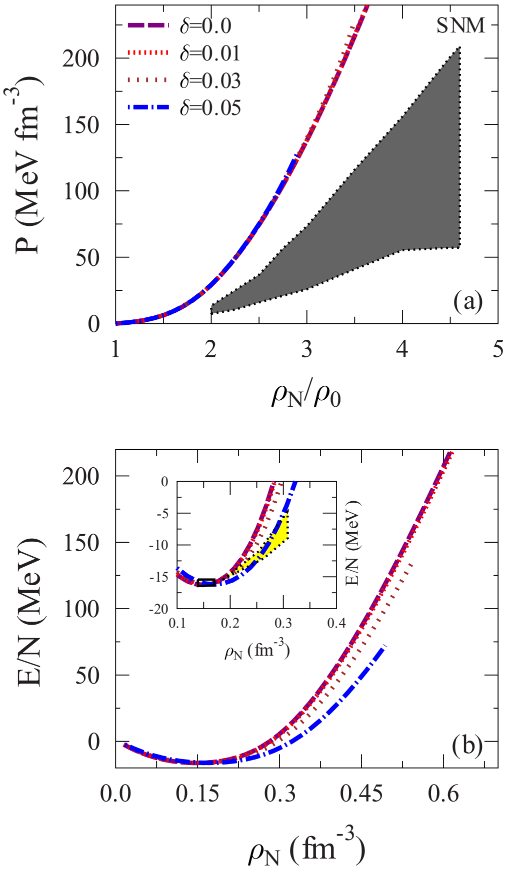

FIG. 3. Similar to Fig. 2 but for the case predicted by the NL3 parameter set.

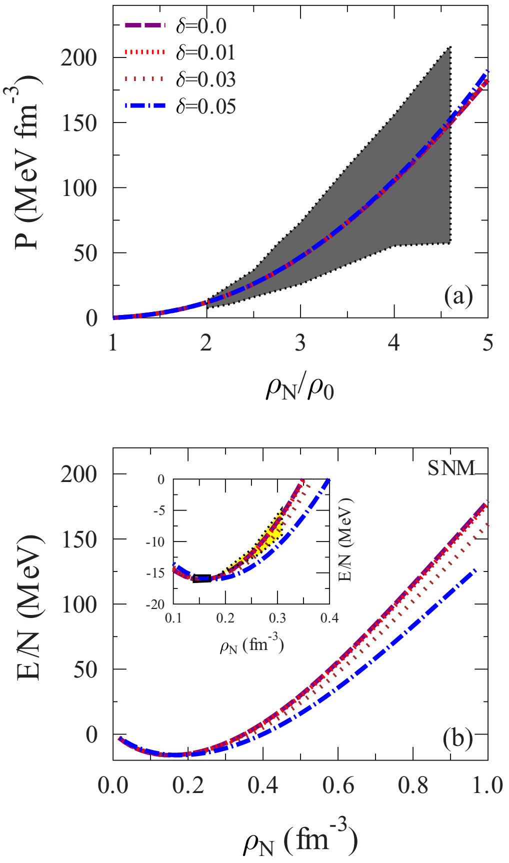

FIG. 4. Similar to Fig. 2 but for the case predicted by the G2 parameter set.

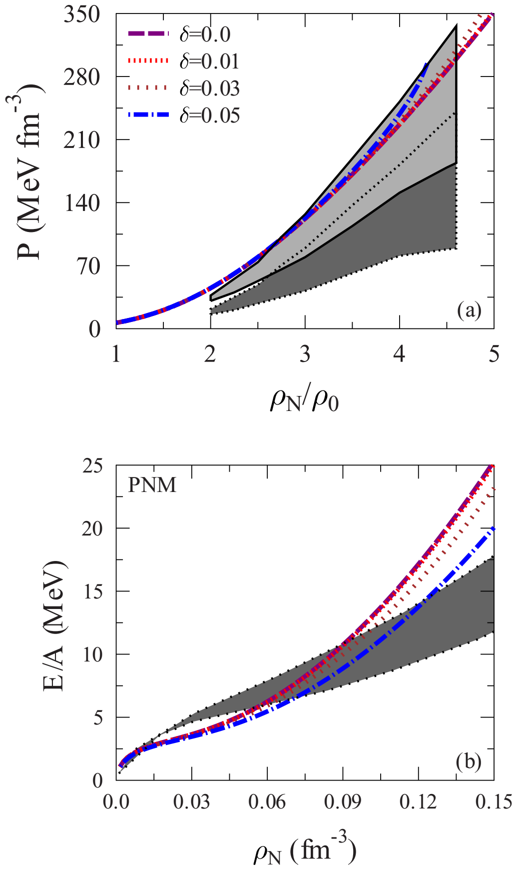

FIG. 5. Similar to Fig. 2 PNM predicted by the TM1 parameter set.

calculations are done for $0 \leqslant \delta \leqslant 0.05$. For comparison, we show the range of EOSs and binding energies extracted from the experimental data and obtained from chiral effective field theory. The shaded areas of the top panels of Figs. 2–7 show the results extracted from heavy-ion experimental data [32], whereas the shaded areas in the insets of Figs. 2–4 show the constraint imposed by the SNM binding energy near twice the saturation density extracted from the FOPI experimental data [33]. Furthermore, the boxed area around ρ_0 indicates the acceptable range of the SNM binding energy around the saturation density extracted from the Bethe-Weizäcker mass formula. The shaded areas in the bottom panels of Figs. 5–7 show the binding energy for PNM at low densities obtained from the chiral effective field theory calculation [34]. Note that the sign of δ has no effect because only δ^2 enters into the EOS. The SNM and PNM EOSs are extracted from the heavy-ion data and the SNM binding energy at saturation density and at twice the saturation density can be used to constrain δ. However, the constraint imposed by the SNM binding energy at saturation density is tighter than the other constraints. Furthermore, the constraint imposed by the SNM binding energy is relatively independent of the EOS stiffness. Conversely, the SNM and PNM EOS extracted from the heavy-ion data, and the binding energy for the PNM at low densities obtained from chiral effective field theory are sensitive to the EOS stiffness. Thus, for very stiff PNM and SNM EOSs, such as those predicted by NL3, the corresponding EOSs are incompatible with those extracted from the heavy-ion data. However, for very soft PNM EOSs, as represented by G2, the binding energy at low densities is incompatible with that obtained from chiral effective field theory.

The figures show that, for relatively soft EOSs such as those obtained by using the TM1 and G2 parameter sets, the Fermi-surface deformation begins to increase the pressure in the region $\rho_N/\rho_0 \gtrsim 4$ if $\delta \gtrsim 0.01$. For stiffer EOSs, the corresponding increase in pressure should start to appear at greater densities. However, we cannot explicitly show this here because, for very stiff PNM and SNM EOSs (e.g., with $\delta = 0.05$), our numerically self-consistent RMF EOS calculation does not converge at relatively high densities and the calculation stops earlier (i.e., around $\rho_N \sim 3\rho_0$). In addition, the NS-matter binding energy at saturation density is only compatible with the corresponding constraint when $\delta \lesssim 0.05$. However, given a NS-matter binding energy of twice the saturation density, the compatibility of the binding-energy predictions of all parameter sets used depends on the stiffness of the EOS but, for $\delta < 0.05$, the corresponding binding energy is quite compatible with the data of Ref. [33]. These results may indicate that the Fermi-surface deformation for nucleons with $\delta \lesssim 0.05$ in nuclear matter remains compatible with all constraints if the EOSs are neither excessively nor insufficiently stiff.

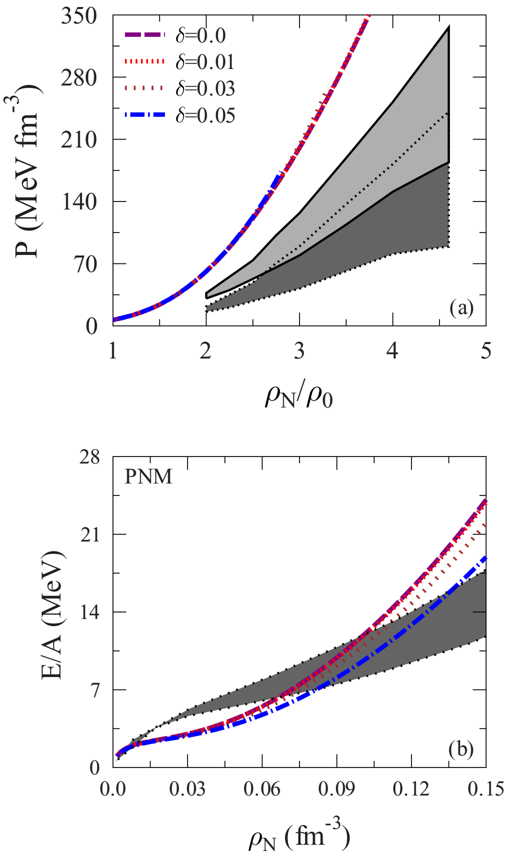

FIG. 6. Similar to Fig. 3 PNM predicted by the NL3 parameter set.

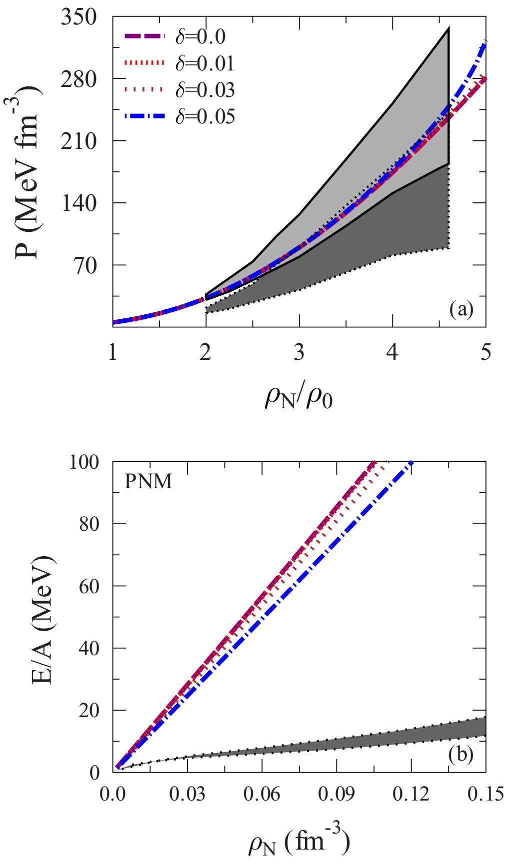

FIG. 7. Similar to Fig. 4 but for the case PNM predicted by the G2 parameter set.

However, a more careful study is required to reach a firmer conclusion because the parameters in the NL3, TM1, and G2 parameter sets are obtained by assuming an isotropic Fermi surface of nuclear matter. In detail, fitting the δ parameter with all the parameters of the RMF models and including isoscalar and isovector tensor terms in the model might provide additional effects. The most crucial SNM property is the binding energy at saturation density (E/N). Other nuclear-matter isoscalar properties at saturation density can be derived from the binding energy $E(\rho)$ as follows:

$$K_0 = 9\rho_0^2 \frac{d^2E(\rho)}{d\rho^2}\bigg|_{\rho=\rho_0}, \quad J_0 = 27\rho_0^3 \frac{d^3E(\rho)}{d\rho^3}\bigg|_{\rho=\rho_0}. \tag{56}$$

Note that, in the isovector sector, the role of the symmetry energy at the saturation density J plays a role similar to that of the binding energy. Other nuclear-matter isovector properties at saturation density can be derived from $J(\rho)$ and are given by the following:

$$L = 3\rho_0 \frac{dJ(\rho)}{d\rho}\bigg|_{\rho=\rho_0}, \quad K_{\rm sym} = 9\rho_0^2 \frac{d^2J(\rho)}{d\rho}^2\bigg|_{\rho=\rho_0},$$

$$K_{asy} = K_{\rm sym} - 6L, \quad K_{{\rm sat},2} = K_{asy} - \frac{J_0}{K_0}L. \tag{57}$$

For completeness, we show in Table I how δ affects the nuclear-matter properties at ρ_0, as predicted when using the TM1 parameter set. The results show that the Fermi-surface deformation for $\delta \leqslant 0.05$ has no significant effect on E/N, K_0, J, L, and $K_{{\rm sat},2}$. The uncertainties in the nuclear-matter EOS are mostly because of the poorly known density dependence of the symmetry energy $J(\rho)$. However, much progress has been reported in this direction (for details, see Ref. [35] and references therein). Reference [36] reports a systematic investigation into the correlation between NS radii and the angular momentum L and the slope of nuclear-matter incompressibility over a wide range of NS EOSs. The correlations between NS core-crust properties and the angular momentum L predicted by different methods have also been studied in Ref. [37] (and references therein). The uncertainties in

TABLE I. Nuclear-matter properties at the saturation density ρ_0 predicted by TM1 with various values for δ. The Fermi momentum k_F, binding energy E, incompressibility coefficient for SNM K_0, symmetry energy J, and other quantities are defined in Eqs. (56) and (57).

δ	0	0.01	0.05
E/N (MeV)	−16.28	−16.28	−16.20
K_0 (MeV)	280.47	280.47	280.47
J (MeV)	−277.05	−277.05	−277.05
L (MeV)	110.61	110.61	110.66
$K_{{\rm sat},2}$ (MeV)	−520.85	−520.86	−521.02

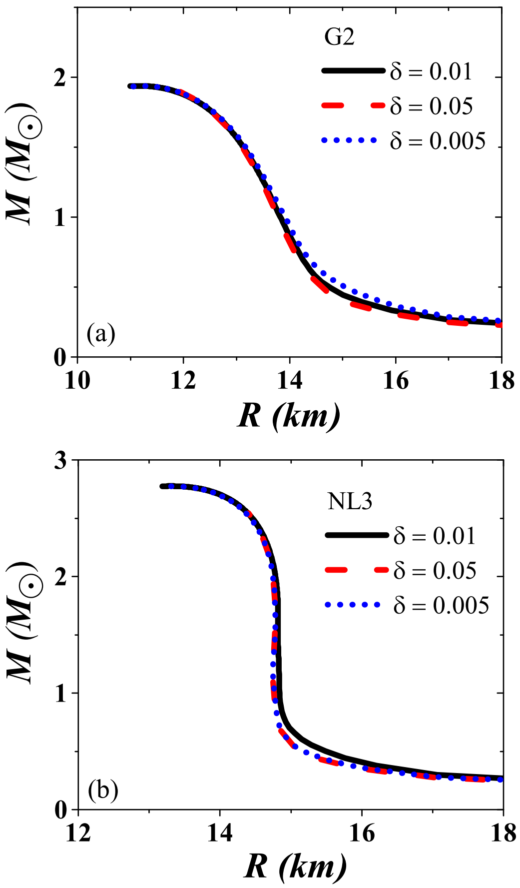

FIG. 8. NS mass M as a function of NS radius R for EOSs using the (a) G2 and (b) NL3 parameter sets. Here we use $\delta = 0.01$, 0.05, and 0.005.

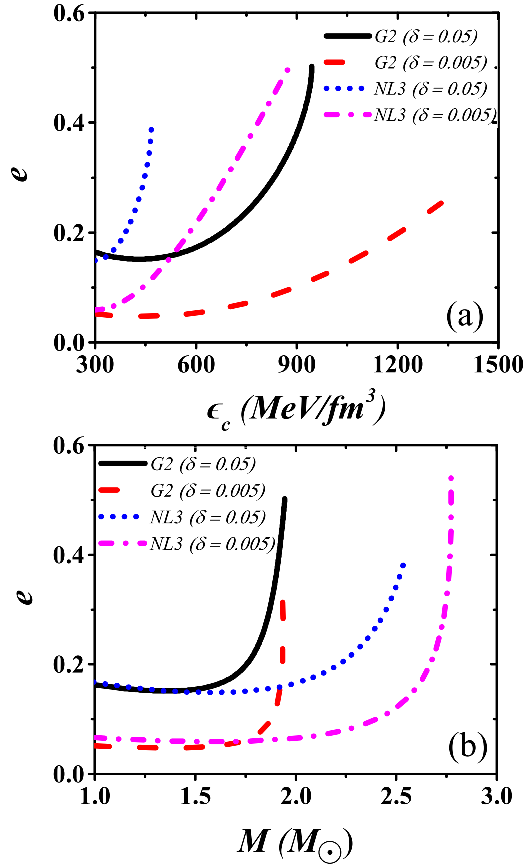

FIG. 9. Relation between eccentricity e for EOSs using the G2 and NL3 parameter sets with (a) the energy density at the NS center (ϵ_c) and (b) M from a NS. Here we use $\delta = 0.05$ and 0.005.

NS radii and crust properties also have been investigated [38]. Finally, Ref. [39] discusses the correlation between the neutron-skin thickness of Pb^{208} and NS tidal deformation and the predicted lower bound for the NS radius based on GW170817 data.

B. Impact of distorted Fermi surface on shape of neutron star

Figure 8 shows the quantity M as a function of the average radius R predicted using the G2 and NL3 parameter sets for $\delta = 0.01, 0.05$, and 0.005. Globally, no significant differences appear in M as a function of R for either parameter set. Some slight differences appear in the curve of M versus R only in the region around $M \lesssim 1M_\odot$. However, the differences not captured in this figure but that significantly affect the NS shape are due to the difference between the equator radius R_e and the polar radius R_p. We discuss this matter later. Note also that, for $\delta = 0.05$, the NS EOSs predicted by both parameter sets converge only up $\rho < 5\rho_0$. Therefore, for both parameter sets, the corresponding largest mass is only close to but never reaches the NS maximum mass predicted in the plot of M versus R. However, we can expect from the M-R trends predicted when using other values of δ for each parameter set that the interpolation of M versus R predicted using $\delta = 0.05$ up to the maximum mass might reach exactly the same maximum mass as obtained when using other δ values. In addition, changes in R_e and R_p should be similar to those predicted when using other values for δ. In the discussion that follows, we use $\delta = 0.05$ and 0.005 to investigate the maximum effect of varying δ.

The most direct information about the shape of a NS is available from the degree of deformation, which is known as the eccentricity e of the NS, where $0 \leqslant e \leqslant 1$. Zero eccentricity ($R_e = R_p$) indicates that the NS does not deform at all (i.e., it remains spherical) and $e = 1$ ($R_e \gg R_p$) indicates that the NS has maximum deformation. Figure 9(a) shows the eccentricity e as a function of energy density at the NS center (ϵ_c). The difference in eccentricity is predicted by using the G2 and NL3 parameter set with $\delta = 0.05$ starts to appear at $\epsilon_c = 250\ \text{MeV/fm}^3$, which corresponds to NSs with $M < 1M_\odot$. This implies that both parameter sets predict significantly different deformations for $\epsilon_c > 250\ \text{MeV/fm}^3$.

As ϵ_c increases, the NL3 parameter set gives NSs that are more easily deformed than those obtained by using the G2 parameter set. The maximum eccentricity e predicted by NL3 is $e \approx 0.5$ and appears at $\epsilon_c \sim 850\ \text{MeV/fm}^3$ where, for the G2 parameter set, the maximum eccentricity $e \approx 0.5$ and appears at $\epsilon_c \sim 940\ \text{MeV/fm}^3$.

Figure 9(b) shows the eccentricity e as a function of NS mass M. For both parameters sets, the eccentricity e

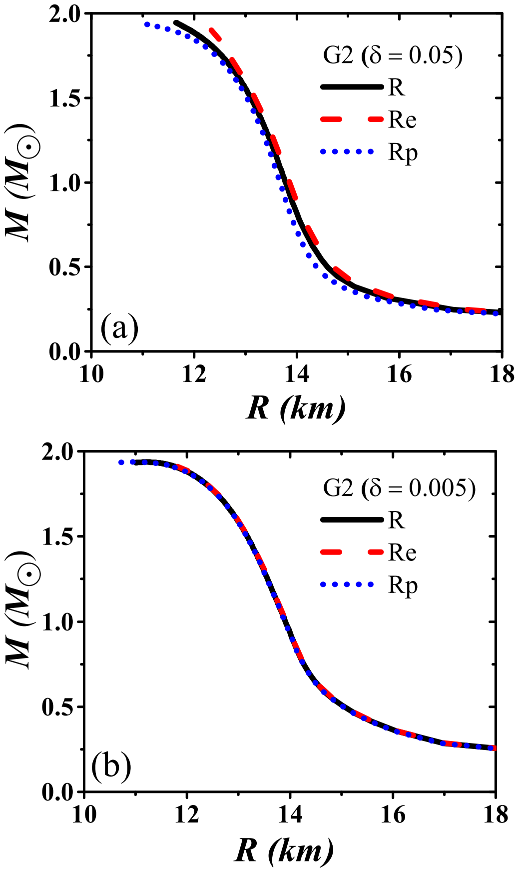

FIG. 10. NS mass M as a function of NS radius R (R, R_e, and R_p) relations using EOSs predicted by using the G2 parameter set with (a) $\delta = 0.05$ and (b) $\delta = 0.005$.

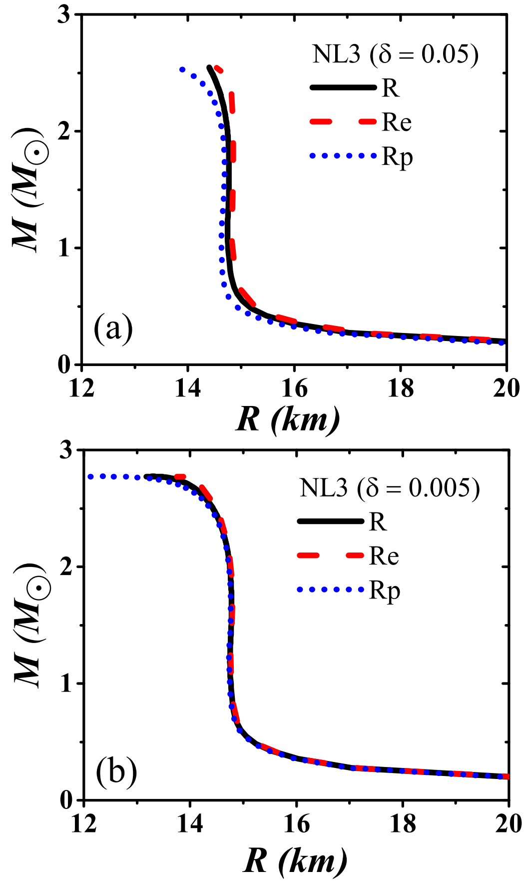

FIG. 11. NS mass M as a function of NS radius R (R, R_e, and R_p) when using EOSs predicted by NL3 parameter set with (a) $\delta = 0.05$ and (b) $\delta = 0.005$.

increases rapidly just before reaching maximum mass and maximizes at maximum mass. When using the G2 parameter set, ϵ_c increases rapidly near the maximum mass $M = 1.94 M_\odot$ whereas, it appears around the maximum mass $M = 2.77 M_\odot$ for $\delta = 0.005$ and $M = 2.54 M_\odot$ for $\delta = 0.05$ when using the NL3 parameter set. Note that the largest mass predicted by both δ parameters of NL3 are not the same because for $\delta = 0.05$, the calculation converges until $M = 2.54 M_\odot$. Figure 9 also shows clearly that the maximum eccentricity e decreases slightly as δ decreases. However, the rate of decrease depends significantly on the EOS stiffness.

For more details, we show in Fig. 10 for G2 and in Fig. 11 for NL3 the NS mass M as a function of average radius R, equatorial radius R_e, and polar radius R_p. The significant differences between R_e and R_p appear only at large NS mass, and the effect is maximal when near the maximum NS mass. This occurs for all parameter sets. Decreasing δ results in a decreasing difference between R_e and R_p, whereas increasing the difference between R_e and R_p results in an increasing deformation of the NS. The latter also can be seen more clearly from two-dimensional plots.

Figure 12 shows two-dimensional plots of R_e and R_p predicted by the G2 and NL3 parameter sets for the maximum pressure at the center of the NSs according to $\delta = 0.05$ converge limits. Here, both the G2 and NL3 parameter sets are using $P_c = 289$ MeV/fm^3 and $P_c = 156$ MeV/fm^3, respectively. The stiffest EOS, here represented by the one of NL3, yield more deformed NSs than the one predicted by the softest EOS, here represented by the EOS of G2. The NS shape predicted by NL3 becomes more oblate than that of G2. Figure 12 also shows that, upon decreasing δ,

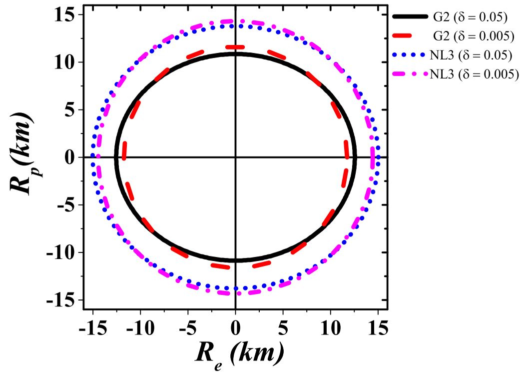

FIG. 12. NS shape for the EOS predicted by parameter set G2 with $\delta = 0.05$ for $M = 1.95 M_\odot$ and with $\delta = 0.005$ for $M = 1.92 M_\odot$; NL3 with $\delta = 0.05$ for $M = 2.54 M_\odot$, and with $\delta = 0.005$ for $M = 2.53 M_\odot$.

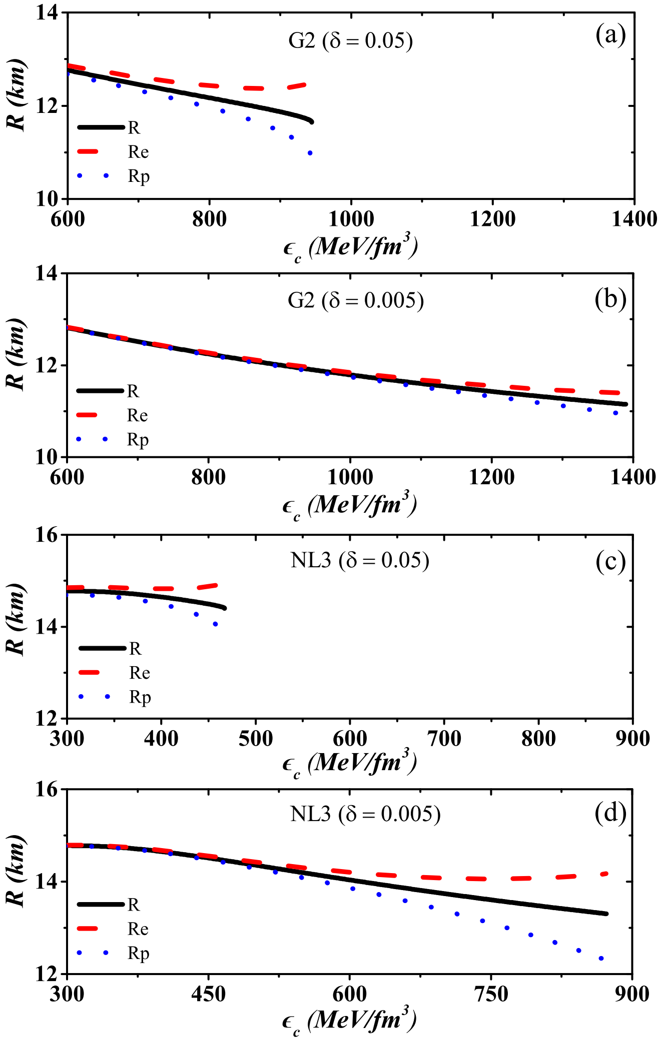

FIG. 13. Spherical radius R as a function of energy density at NS center ϵ_c and for (a) G2 with $\delta = 0.05$, (b) G2 with $\delta = 0.005$, (c) NL3 with $\delta = 0.05$, and (b) NL3 with $\delta = 0.005$.

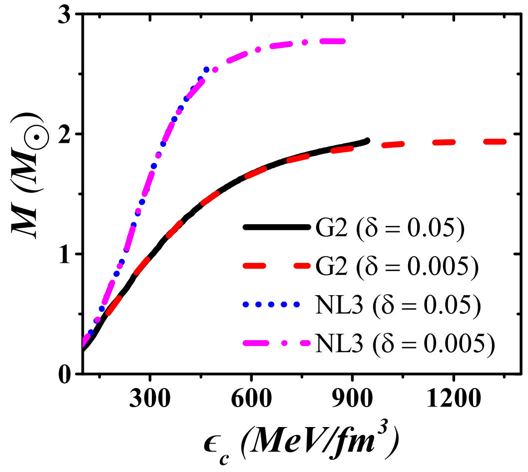

FIG. 14. Mass as a function of ϵ_c for G2 and NL3 parameter sets with $\delta = 0.005$ and $\delta = 0.05$.

R_e becomes slightly smaller and R_p becomes slightly larger than their initial values, which means that the stiffness of the corresponding EOS changes the NS shape more significantly than increasing δ in the range of allowed values.

In addition, we show the equatorial and polar radii R_e and R_p as functions of ϵ_c in Fig. 13. The NS deformation because of differences between R_e and R_p is clearly more significant in the region with relatively large ϵ_c or large NS mass. The magnitude of NS deformation depends on two factors: the EOS stiffness and the value of δ. For completeness, we also provide the plot of NS mass as the function of ϵ_c for G2 and NL3 parameter sets with $\delta = 0.005$ and $\delta = 0.05$. in Fig. 14 to emphasize this finding.

To understand these results, we plot in Fig. 15 the source of the anisotropic pressure that is responsible for NS deformation (i.e., NS σ_c) as a function of R_e and R_p. The value of σ_c increases significantly after reaching the critical values for R_e and R_p. Near these critical radii, the NS mass is large and σ_c increases up to the maximum value for the maximum mass. Note that, for each parameter set, the slope of σ_c with respect to both radii depends slightly on δ. In addition, the increase in σ_c predicted by NL3 starts at a larger critical radius compared with the corresponding critical radius for G2. This indicates that the behavior of σ_c depends significantly on the EOS stiffness and only slightly on δ.

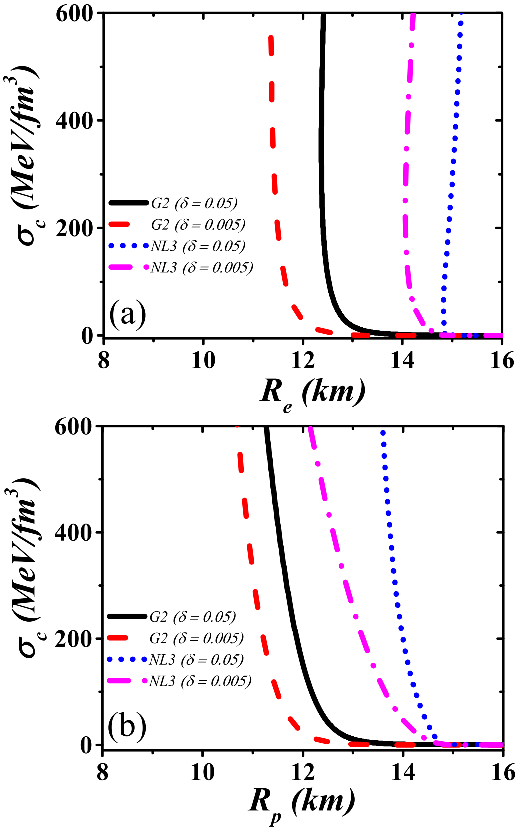

FIG. 15. Anisotropic factor σ_c at the NS center as a function of NS star radius (a) R_e and (b) R_p obtained by using the EOSs predicted by using the G2 and NL3 parameter sets with $\delta = 0.05$ and $\delta = 0.005$.

Note that the difference in Fermi-surface deformation and the difference with the pure slow-rotation approach [23,24] lies in the multipole expansion of the energy-momentum tensor. In the slow-rotation approach, the baryon number density, the mass-energy density, and the fluid pressure are affected by the rotation because the rotation is the agent of deformation. Therefore, for slow rotation, both energy density and pressure in the energy-momentum tensor acquire terms because of the multipole expansion. However, for deformation caused by Fermi-surface distortion, the anisotropic pressure factor is the only agent of deformation. Therefore, only the corresponding pressure in the energy-momentum tensor acquires terms due to multipole expansion. The latter is quite similar to the deformation caused by a magnetic field [25]. Furthermore, in our calculation, the angular velocity is not included in the Schwarzschild metric as is done in the calculation of deformation because of slow rotation [23,24]. Therefore, the deformation in this calculation is purely from the anisotropic momentum distribution. The global impact is also different, and the deformation caused by slow rotation and magnetic field tends to make the NS shape more prolate, whereas the deformation due Fermi-surface deformation tend to make the NS shape more oblate.

IV. CONCLUSIONS

We study how the distortion of the Fermi surface affected the SNM, PNM, and NS matter. We applied various constraints, such as the binding energy at saturation density extracted from the Bethe-Weizäcker mass formula, the binding energy at about twice the saturation density extracted from FOPI experimental data, and the EOSs at moderate densities, which are extracted from heavy-ion experimental data to verify the sensitivity of the deformation parameter δ to the corresponding EOS and binding energy and to estimate the allowed range of δ. The results indicate that the SNM binding energy can impose $\delta \lesssim 0.05$. The impact of δ on the stiffness of the SNM and PNM EOS starts to appear when $\delta \gtrsim 0.01$. However, for $\delta \gtrsim 0.05$, the EOSs in our PNM, SNM, and NS matter calculations stop at relatively moderate densities depending on the EOS stiffness. This result is attributed to the lack of convergence in our calculation at high densities. Therefore, for $\delta \gtrsim 0.05$, the calculated result is close but never reaches the NS maximum mass. We use $\delta = 0.005$ and $\delta = 0.05$ to study the NS properties. If the Fermi surface is distorted, then the NS can be deformed into an oblate form. The corresponding NS deformation is manifested in the difference between R_e and R_p, which is more significant for a relatively large ϵ_c or for M near the maximum mass. The corresponding deformation depends on two factors: the stiffness of the EOS (dominant factor) and the value of δ (secondary factor). The source of this deformation is the anisotropic pressure in the NS center because of the distorted Fermi surface and that significantly increases near the maximum NS mass.

ACKNOWLEDGMENTS

A.S. and R.R. were supported by Direktorat Riset dan Pengabdian Masyarakat (DRPM) Universitas Indonesia through PITTA Grants No. 2230/UN2.R3.1/HKP.05.00/2018 and No. 2231/UN2.R3.1/HKP.05.00/2018. A.S. has also funded by Direktorat Riset dan Pengabdian Masyarakat (DRPM) Universitas Indonesia through Q1Q2 Grant No. NKB-0267/UN2.R3.1/HKP.05.00/2019.

[1] J. M. Lattimer, Annu. Rev. Nucl. Part. Sci. **62**, 485 (2012).
[2] N. Chamel, P. Haensel, J. L. Zdunik, and A. F. Fantina, Int. J. Mod. Phys. E **22**, 1330018 (2013).
[3] D. Lonardoni, A. Lovato, S. Gandolfi, and F. Pederiva, Phys. Rev. Lett. **114**, 092301 (2015).
[4] Y. Yamamoto, T. Furumoto, N. Yasutake, and Th. A. Rijken, Phys. Rev. C **90**, 045805 (2014).
[5] A. V. Astashenok, S. Capozziello, and S. D. Odintsov, Phys. Rev. D **89**, 103509 (2014).
[6] S. Weissenborn, I. Sagert, G. Pagliara, M. Hempel, and J. Schaffner-Bielich, Astrophys. J. Lett. **740**, L14 (2011).
[7] A. Sulaksono and B. K. Agrawal, Nucl. Phys. A **895**, 44 (2016).
[8] X.-T. He, F. J. Fattoyev, B.-A. Li, and W. G. Newton, Phys. Rev. C **91**, 015810 (2015).
[9] E. Berti *et al.*, Classical Quantum Gravity **32**, 243001 (2015).
[10] I. Ia. Pomeranchuk, Sov. Phys. JETP **35**, 524 (1958).
[11] J. Quintanilla, M. Haque, and A. J. Schofield, Phys. Rev. B **78**, 035131 (2008).
[12] S. S. Pankratov, M. Baldo, and M. V. Zverev, Pis'ma Zh. Eksp. Teor. Fiz. **106**, 689 (2017) [JETP Lett. **106**, 720 (2017)].
[13] C. Zhao, L. Jiang, X. Liu, W. M. Liu, X. Zou, and H. Pu, Phys. Rev. A **81**, 063642 (2010).
[14] G. B. Partridge, W. Li, Y. A. Liao, R. G. Hulet, M. Haque, and H. T. C. Stoof, Phys. Rev. Lett. **97**, 190407 (2006).
[15] A. Sedrakian, J. Mur-Petit, A. Polls, and H. Müther, Phys. Rev. A **72**, 013613 (2005).
[16] A. Rodriguez-Prieto, A. Bergara, V. M. Silkin, and P. M. Echenique, Phys. Rev. B **74**, 172104 (2006).
[17] H. Müther and A. Sedrakian, Phys. Rev. Lett. **88**, 252503 (2002).
[18] H. Müther and A. Sedrakian, Phys. Rev. C **67**, 015802 (2003).
[19] T. Frick, H. Müther, and A. Sedrakian, Phys. Rev. C **65**, 061303(R) (2002); **69**, 049802 (2004).
[20] E. S. Corchero, Classical Quantum Gravity **15**, 3645 (1998); Astrophys. Space Sci. **259**, 31 (1998).
[21] T. Mart and A. Sulaksono, Phys. Rev. C **87**, 025807 (2013); Suparti, A. Sulaksono, and T. Mart, *ibid.* **95**, 045806 (2017).
[22] W. Greiner and J. A. Maruhn, *Nuclear Models* (Springer, Heidelberg, 1995).
[23] J. B. Hartle, Astrophys. J. **150**, 1005 (1967).
[24] J. B. Hartle and K. S. Thorne, Astrophys. J. **153**, 807 (1968).
[25] R. Mallick and S. Schramm, Phys. Rev. C **89**, 045805 (2014).
[26] C. J. Horowitz and J. Piekarewicz, Phys. Rev. Lett. **86**, 5647 (2001).

[27] N. K. Glendenning, *Compact Stars, Nuclear Physics, Particle Physics, and General Relativity* (Springer, New York, 1997).

[28] E. Berti, F. White, A. Maniopoulou, and M. Bruni, Mon. Not. R. Astron. Soc. **358**, 923 (2005).

[29] G. A. Lalazissis, J. König, and P. Ring, Phys. Rev. C **55**, 540 (1997).

[30] Y. Sugahara and H. Toki, Nucl. Phys. A **579**, 557 (1994).

[31] R. J. Furnstahl, B. D. Serot, and H. B. Tang, Nucl. Phys. A **598**, 539 (1996); **615**, 441 (1997).

[32] P. Danielewicz, R. Lacey, and W. G. Lynch, Science **298**, 1592 (2002).

[33] A. Le Févre, Y. Leifels, W. Reisdorf, J. Aichelin, and Ch. Hartnack, Nucl. Phys. A **945**, 112 (2016).

[34] T. Krüger, I. Tews, K. Hebeler, and A. Schwenk, Phys. Rev. C **88**, 025802 (2013).

[35] J. Piekarewicz, F. J. Fattoyev, and C. J. Horowitz, Phys. Rev. C **90**, 015803 (2014).

[36] N. Alam, B. K. Agrawal, M. Fortin, H. Pais, C. Providência, A. R. Raduta, and A. Sulaksono, Phys. Rev. C **94**, 052801(R) (2016).

[37] H. Pais, A. Sulaksono, B. K. Agrawal, and C. Providência, Phys. Rev. C **93**, 045802 (2016).

[38] M. Fortin, C. Providência, A. R. Raduta, F. Gulminelli, J. L. Zdunik, P. Haensel, and M. Bejger, Phys. Rev. C **94**, 035804 (2016).

[39] F. J. Fattoyev, J. Piekarewicz, and C. J. Horowitz, Phys. Rev. Lett. **120**, 172702 (2018).